Synchrotron X-ray Scattering Studies of Crystallization of Poly(ether–ether–ketone) from the Glass and Structural Changes during Subsequent Heating–Cooling Processes

Alain M. Jonas,† Thomas P. Russell, and Do Y. Yoon*

IBM Almaden Research Center, 650 Harry Road, San Jose, California 95120

Received May 4, 1995; Revised Manuscript Received September 5, 1995®

ABSTRACT: The evolution of structural parameters characterizing the semicrystalline morphology of poly(aryl–ether–ether–ketone) (PEEK), and its blends with poly(aryl–ether–imide) (PEI), has been determined as a function of temperature by means of small-angle (SAXS) and wide-angle (WAXS) X-ray scattering studies, using synchrotron radiation. By comparing the behavior of initially amorphous samples continuously heated in the beam and samples heated and cooled below and above their annealing temperature, a complete picture is drawn of the morphological changes occurring during the cold crystallization and subsequent heating–cooling of PEEK. Upon crystallization of an amorphous sample, new lamellae are progressively inserted in the free space left between existing ones. No decrease of the lamellar thickness is evident during this insertion mechanism. When the polymer is cooled below its last annealing temperature T_c, only reversible morphological changes occur, which can be explained quantitatively by the effects of thermal expansion, provided one takes into account the existence of strains in the crystalline lamellae created by their coupling to the noncrystalline interlamellar regions. When the polymer is heated above T_c, "irreversible" changes occur in the average thickness of the lamellar crystals and of the interlamellar noncrystalline regions, in the perfection of the crystals, and in the crystalline density. Cold-crystallized samples are shown to comprise a single lamellar population which undergoes a rapid melting–recrystallization process above T_c. The double melting behavior of cold-crystallized PEEK results from this melting–recrystallization mechanism.

Introduction

The morphology and properties of a semicrystalline polymer depend on its thermal history. Therefore, when studying the morphology, changes in the structure as a function of the crystallization conditions and subsequent thermal treatments must be considered. Moreover, any technique where the sample is heated in order to get structural information can itself induce changes in the sample. This, for example, is encountered in differential scanning calorimetry (DSC), where multiple melting peaks are often seen. It is usually difficult to ascertain whether the endotherms are due to entities present in the original sample or to ones generated during the heating in the DSC cell. A more practical issue is to know whether the structure of a polymer is modified during a cooling after crystallization, or how the structure is modified by short exposures to temperatures higher than the crystallization temperature T_c.

In this article, a description of the crystallization of poly(ether–ether–ketone)[1] (PEEK) from the glass, and of the structural changes occurring during subsequent thermal treatments, is discussed. Real-time small-angle X-ray scattering (SAXS) and wide-angle X-ray scattering (WAXS) at a synchrotron radiation source, in conjunction with DSC and dynamical mechanical analysis (DMA), have been used to provide structural details. Similar studies on poly(ethylene terephthalate)[1] (PET) have been reported elsewhere.[2] While most of the results presented here deal with PEEK, some studies on mixtures of PEEK with poly(ether imide)[1] (PEI) will be discussed. PEI is miscible in all proportions with amorphous PEEK.[3] Since the glass transition temperature (T_g) of PEI (217 °C) is much higher than the T_g of PEEK (140 °C), the presence of PEI in the initially amorphous blends narrows the temperature interval where crystallization can occur, increasing the minimum possible T_c, based simply on composition. Upon PEEK crystallization, the PEI is expelled from the crystalline lamellae; at the outcome of the crystallization, PEI is mostly located in interspherulitic and interfibrillar regions,[4–6] with still a small amount of PEI being trapped in interlamellar regions.[6] In the present study, we will examine the way PEI affects the subsequent structural evolution of PEEK.

PEEK has been studied extensively as a prominent high performance polymer,[7] and it typifies aromatic semicrystalline polymers. It exhibits multiple melting peaks in DSC experiments, which have been the source of much controversy.[8–15] There have been previous studies using synchrotron radiation and other techniques on the development and evolution of the semicrystalline morphology in PEEK, PET, and other aromatic polymers. Since differences in the morphology could arise from differences in the thermal treatment of the samples, it is necessary to pay close attention to the mode of preparation and thermal history of the samples. Failure to do so has led to unnecessary confusion in the literature.

During *isothermal crystallization of aromatic polymers from the glass or from the melt*, a decrease of the long period (i.e., the average distance between the lamellar crystals) is usually observed with time.[16–21] This has been attributed to a crystallization process where new lamellae grow in-between existing lamellae, though progressive flattening of initially bended lamellae (decreasing corrugation of lamellae over time) has also been proposed.[16,21] Experimental results on PEEK also indicate that the lamellar thickness is independent of time during the crystallization.[20] Even still, some authors[18,19,22] suggest that a dual population of lamellar thicknesses exists, where thinner lamellae are inserted between the existing lamellae in the last stages of the

† Present address: Laboratoire des Hauts Polymères, Université Catholique de Louvain, Place Croix du Sud, 1, B-1348 Louvain-la-Neuve, Belgium (E.U.).

® Abstract published in *Advance ACS Abstracts,* November 1, 1995.

0024-9297/95/2228-8491$09.00/0

crystallization. Such a dual population of crystal thicknesses have been used to account for the double-melting behavior of PEEK and other aromatic polymers.

Recently, Krüger and Zachmann[23] performed an extensive set of SAXS, WAXS, and DSC measurements on PEEK, where PEEK was cooled decrementally *by steps from the melt to successively lower crystallization temperatures*. The results indicated that during the holding time at each temperature a new lamellar population, characterized by a smaller thickness than the existing lamellae, was formed. Upon heating, the melting of each population was detected by a sudden increase in the long period, a decrease of the crystallinity, and a small melting endotherm in the DSC trace. In addition, no recrystallization was observed, which is in keeping with a previous interpretation of DSC results by Chang.[13] Cheng *et al.*[8] observed that when crystallizing PEEK at high temperatures from the melt, a significant part of the sample only crystallizes during the cooling following the isothermal crystallization. Hence, there is little doubt that lamellar populations of different thicknesses can coexist in PEEK crystallized in a stepwise manner, which leads to a multiple melting behavior. These arguments are similar to those proposed for the partial melting of polyethylene.[24] However, the location of the thinner lamellae remains open to discussion. Krüger and Zachmann[23] suggest that they are located between thicker lamellae. Verma *et al.*,[25] however, indicate that the thinner lamellae form in separate lamellar stacks, in agreement with electron microscope experiments[26] that reveal the existence of relatively large amorphous regions in PEEK samples crystallized from the melt at high temperatures (typically 310–330 °C). Another point that remains to be established is whether all the secondary melting peaks observed in stepwise-cooled PEEK originate from the same mechanism, given the observations reported in the next paragraph.

Other results on PEEK provide evidence that double-melting peaks can be obtained by *isothermal crystallization from the melt*. Upon heating such PEEK samples, Hsiao *et al.*[20,22] noticed a two-stage increase of the long period with temperature. The slower first stage was interpreted as originating from thermal expansion, while the second was interpreted as resulting from the melting of the thinner lamellae of a hypothesized dual lamellar population. A progressive thickening of the remaining larger lamellae was also suggested, displacing the final melting of the sample to higher temperatures. Support to these interpretations was sought from DSC[8] and electron microscopy[12,15] experiments performed on PEEK samples crystallized *at high temperatures* (above ~300 °C). Again, there are divergences between authors concerning the location of the thinner lamellae, either in separate stacks[25] or inserted in stacks of thicker ones.[19] There is also disagreement as to whether the two different lamellar populations grow simultaneously[15] or in series.[8,12] The situation is further confused by the existence of different morphological forms of PEEK at high temperatures,[26,27] and by the possible thermal degradation of PEEK held for long times at high temperatures, even in nitrogen.[28,29]

When *crystallized from the glassy state*, aromatic polymers generally exhibit a multiple melting behavior in subsequent DSC scans as well. Usually, a small melting endotherm is first observed a few degrees above the prior crystallization or annealing temperature T_c. A larger melting endotherm appears at higher temperatures, which is essentially independent of T_c. This behavior was investigated for PET by Gehrke *et al.*,[30] using synchrotron radiation. It was shown that, below T_c, the variations of the SAXS signal with temperature could be explained by thermal expansion, coupled with a small amount of premelting near T_c. Above T_c, extensive melting followed by recrystallization was observed. This last phenomenon could only be observed at high temperatures, near the final melting endotherm of PET, where the recrystallization rate was slow enough. These results support the arguments of Holdsworth *et al.*,[31] where the first melting peak was attributed to the onset of melting of crystals generated at T_c, the major part of this melting being masked by the simultaneous recrystallization. The last melting peak is due to the final melting of the fully-recrystallized structure. From DSC and/or SAXS results, it has been suggested by various authors that a similar melting–recrystallization mechanism is responsible for the double-melting behavior of cold-crystallized PEEK.[10,11,23] But here again, some authors suggest from DSC and electron microscope experiments[8,9,12,18] that the two melting endotherms arise from two distinct populations of lamellae having different stabilities, though some partial melting and recrystallization are frequently acknowledged. Thus, it is not clear whether the first melting endotherm corresponds to the melting of a portion of the crystals initially present, or to the beginning of the melting–recrystallization of *all* the original crystals. In this work, real-time SAXS and WAXS studies have been performed to address the origin of this double-melting behavior of cold-crystallized PEEK.

Experimental Section

PEEK (grade 150P) was used as received from ICI. The molecular weights determined by size exclusion chromatography were[32] $M_n = 10\,300$ and $M_w = 26\,800$. The PEI powder (Ultem 1000), received from General Electric Co., was used as received. PEEK/PEI blends were prepared as described elsewhere.[6] The powders were compression-molded at 400 °C for 10 min in a vacuum-sealed container into ~400 μm thick films and then quenched in water. The films were transparent and showed no trace of crystallinity or orientation as measured by wide-angle X-ray diffraction.

X-ray scattering measurements were performed on beamline I-4 at the Stanford Synchrotron Radiation Laboratory (SSRL). For SAXS measurements, the photodiode array detector was located ~50 cm from the sample. Details of the experiment and data correction are described elsewhere.[33] A simple, angularly independent background was used to approximate thermal density fluctuation scattering, due to the limited angular range measured.

For WAXS measurements, the detector was placed closer to the sample, at an inclination of ~20° relative to the horizontal plane. The detector covered the range $15° < 2\theta < 24°$, where 2θ is the angle between the incident and diffracted beams. This was sufficient to observe the three strongest reflections of PEEK, i.e., (110), (111), and (200). The angular range of the detector was calibrated by comparison of the diffraction profiles of a series of well-crystallized PEEK/PEI samples obtained in this geometry to those measured with a classical laboratory diffractometer.[6]

The temperature of the sample was controlled by a Mettler hot stage operating between 50 and 300 °C. Various thermal cycles were applied to the samples, with heating and cooling rates of 3 °C min^{-1}. For each thermal cycle, a new sample was used. The acquisition time for each scattering curve was 1 min.

Differential scanning calorimetry (DSC) was performed at 3 °C min^{-1} heating in a "Thermal Analysis" calorimeter calibrated with indium and zinc.

Dynamical mechanical analysis (DMA) measurements were performed on a Rheometrics RSA II in tension mode. Experimental parameters were as follows: frequency, 1 Hz; heating rate, 3 °C min^{-1}; dynamic deformation, 0.04% below 160 °C, 0.2% above 160 °C.

Data Analysis

From the SAXS data the long period, L, corresponding to the average center-to-center distance between adjacent lamellae, was determined from the peak position in the Lorentz-corrected data. The total integrated scattering or invariant, Q, is given by:

$$Q = K\int_0^\infty q^2 I(q)\, dq$$

where K is a constant and q is the length of the scattering vector given by $q = (4\pi/\lambda)\sin\theta$, where λ is the wavelength and 2θ is the scattering angle. The invariant is related to the difference between the electron densities of the crystalline and noncrystalline regions, $\rho_c - \rho_a$, the linear crystallinity, $\phi_{c,lin}$ (the relative volume fraction of lamellae within the lamellar stacks), and the width of a linearly-varying density transition layer between the crystalline and noncrystalline regions, d, by:

$$Q \propto \phi_s\left(\phi_{c,lin}(1-\phi_{c,lin}) - \frac{d}{3L}\right)(\rho_c - \rho_a)^2$$

where ϕ_s is the volume fraction of lamellar stacks. The total crystallinity of a sample is, therefore, $\phi_s\phi_{c,lin}$. For samples with narrow interfacial width, as is the case here,[6] then:

$$Q \propto \phi_s(\phi_{c,lin}(1-\phi_{c,lin}))(\rho_c - \rho_a)^2 \qquad (1)$$

Since the data were not placed in asbolute units, Q has only a relative meaning in this work.

The average lamellar thickness, L_c, was obtained from the one-dimensional correlation function ($\gamma_1(r)$), computed by Fourier transformation of the Lorentz-corrected scattering. Before Fourier transformation, the data were extrapolated in the high-q range using Porod's law.[34] Rigorously, a prior knowledge of the linear crystallinity is required to determine accurately the values of L_c from the correlation function.[35] However, a reasonable estimate of L_c can be obtained by computing the distance r corresponding to the intersection between the slope of the self-correlation triangle with the horizontal line passing through the first minimum of the correlation function.[35] Then, from the ratio of L_c and L, one obtains an estimate for $\phi_{c,lin}$. Only general trends will be considered in this paper, owing to the simplicity of the analysis. Note that, *a priori*, the SAXS data could have been interpreted differently. Due to Babinet's reciprocity theorem, the value measured for the crystal thickness could have been assigned to the noncrystalline interlayer, and *vice versa*. Such a "reverse" picture has gained in popularity recently.[5,22,25] Reasons for our selecting the smaller distance as being the crystal thickness are given in the Discussion section.

For each WAXS scattering curve, the (110), (111), and (200) reflections were measured and used to determine the unit cell dimensions and crystal density ρ_c. The precision to which the c-axis can be determined is low since only one (hkl) reflection of nonzero l is used. This uncertainty will, also, propagate to the determination of the crystal density. However, since the variation with crystallization conditions in the c-axis dimension is much less than that for the a or b cell dimensions,[36] most conclusions on the evolution of ρ_c with crystallization conditions can be drawn from an examination of a and b only.

By comparing the WAXS under the crystalline reflections, $I_c(q)$, to the overall diffracted intensity, $I(q)$, one can obtain a measure of the mass fraction of crystalline material in the sample. Since our measurements extended over a finite q range, the crystallinity measured in this manner is only approximate. Moreover, distorsions to the crystal lattice, thermal disorder, and other factors cause a reduction of $I_c(q)$ that results in underestimating the crystallinity. Hence, the value determined shall be termed the apparent crystallinity, A_c, which is given by:

$$A_c = k\frac{\int_{q_1}^{q_2} I_c(q)\, q^2\, dq}{\int_{q_i}^{q_2} I(q)\, q^2\, dq} \qquad (2)$$

This apparent crystallinity is related to the actual volume of crystallinity in the sample, ϕ_c, by:

$$A_c = f(T)\,\phi_c = f(T)\,\phi_s\phi_{c,lin} \qquad (3)$$

where $f(T)$ is a temperature-dependent factor taking into account the deviations mentioned above and minor corrections to translate mass to volume crystallinity. The value of k in eq 2 was adjusted in order to match the A_c values obtained at room temperature on a series of well-crystallized PEEK samples, with ϕ_c values determined on the same samples by application of the Ruland's analysis on data acquired with a laboratory diffractometer in a much wider angular range.[6] Hence, A_c exactly corresponds to the real crystallinity ϕ_c when the internal disorder of the crystals is similar to that of the crystals of the standard samples at room temperature. In other cases, it provides a qualitative measure of ϕ_c.

Results

The samples were subjected to various thermal histories. We will first present the results obtained when simply heating and cooling well-crystallized samples below their crystallization temperature. Next, we will present data acquired while continuously heating initially amorphous samples. Finally, we will combine both types of experiments, by making repeated {heating; holding at T_c; cooling} cycles on the samples, while gradually incrementing T_c.

A. Reversible Behavior. To obtain the variations of L, L_c, Q, ρ_c, and A_c with temperature supposedly in the absence of structural changes, experiments were performed on PEEK samples prepared by crystallization from the glass for 10 h in nitrogen at T_c = 280 or 320 °C and, then, quenched in air. DSC thermograms of these samples are featureless below T_c, except for the glass transition around 150–160 °C. These samples have then been heated in the beam from 30 °C to T_c − 20 °C or T_c − 40 °C, cooled to room temperature, and then heated again. The results are shown in Figures 1 and 2, where solid circles denote the results for the first heating run, open circles for cooling, and filled squares for the second heating. Within experimental error, heating and cooling runs give the same results; i.e., the variation of the structural parameters with temperature is reversible below T_c.

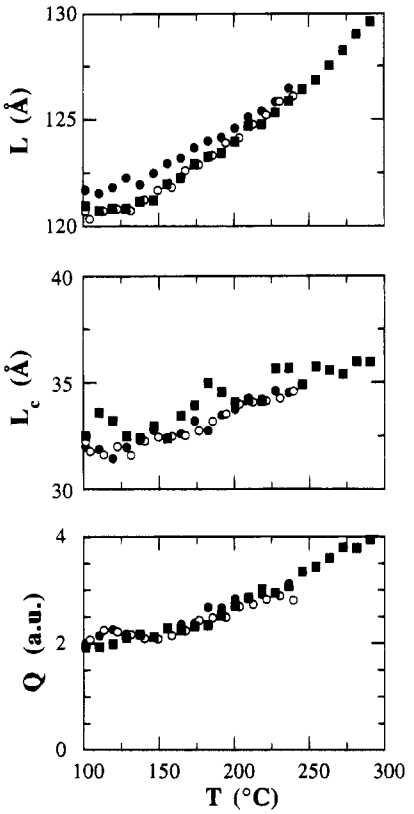

Figure 1. Reversible evolution with temperature of the SAXS long period (L), the average lamellar thickness (L_c), and the SAXS invariant (Q), for a well-crystallized PEEK sample heated, cooled, and heated again at 3 °C min^{-1} below its crystallization temperature (sample initially annealed 10 h at 280 °C from the glass). Filled circles: first heating scan; open circles: cooling scan; filled squares: second heating scan.

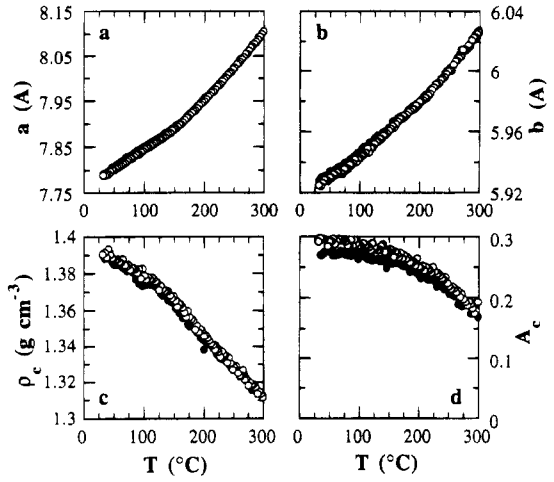

Figure 2. Reversible evolution with temperature of the unit cell dimensions along [100] (a) and [010] (b), of the unit cell density (ρ_c) (c), and of the apparent crystallinity (A_c, eq 2) (d), for a well-crystallized PEEK sample heated and cooled at 3 °C min^{-1} below its crystallization temperature (sample initially annealed 10 h at 320 °C from the glass). Filled symbols: heating scan; open symbols: cooling scan.

From the WAXS data, the thermal expansion coefficient for the volume of the unit cell ($\alpha_{v,c}$) would amount to 2.5 × 10^{-4} °C^{-1} above the PEEK glass transition temperature (T_g = 140−150 °C), and to 1.47 × 10^{-4} °C^{-1} below T_g. These are typical figures for the crystal thermal expansion coefficient of semicrystalline polymers.[37] Assuming that the variation of the invariant Q during these experiments is also due solely to thermal expansion, it is then possible to compute the volume expansion coefficient of the interlamellar amorphous regions ($\alpha_{v,a}$) by using eq 1, together with the previously determined value of $\alpha_{v,c}$. The result is $\alpha_{v,a}$ = 7.3 × 10^{-4} °C^{-1} above T_g. This value can be compared to 6.7 × 10^{-4} °C^{-1} reported by Zoller *et al.*[36] for the volume thermal expansion of molten PEEK. Given the relatively low precision on the invariant, the agreement is quite good and confirms that, indeed, the variations observed for Q and ρ_c can be explained solely by thermal expansion.

Of particular interest here is the observation that $\alpha_{v,c}$ is different below and above the glass transition of the amorphous regions of the polymer (Figure 2). It is difficult to believe that the amplitude of atomic vibrations in the crystals depends on the mobility of the chains in the adjacent amorphous regions. Therefore, above T_g, another mechanism superimposed to the anharmonicity of the atomic vibrations is controlling the volume of the unit cell of the crystal. The only possibility is that the difference of thermal expansion between the amorphous and crystalline regions creates compressive stresses in the crystals during the cooling following crystallization. Upon heating, the progressive modification of these differential stresses results in a larger expansion of the unit cell, the effects being reversible with temperature. This indicates that the thickness of the lamellae is much too small to allow the dissipation of the constraints generated at the crystal surface due to the connectivity of the chains. The effect appears dominantly on the a-axis ([100] direction), along which the interchain forces are the weakest.[38] Note that a similar experimental observation was made previously on drawn PEEK films.[39]

We now turn to the variation of the apparent crystallinity with temperature. A_c decreases by slightly more than 35% during heating from 30 to 300 °C, most of the decrease occurring above T_g. Referring to eq 2, the decrease of A_c may be due to a decrease of $\phi_{c,lin}$, ϕ_s, or $f(T)$. As a decrease of ϕ_s would similarly decrease Q, this possibility can be ruled out. A limited decrease of $\phi_{c,lin}$ would not significantly alter Q (eq 1); however, it would correspond to a significant decrease of L_c versus L. Since this is not observed, the variations of A_c with temperature must be attributed to variations of the disorder factor $f(T)$. The gradual decrease of $f(T)$ and A_c below T_g is due to atomic vibrations of increasing amplitude (Debye−Waller factor). However, these vibrations should not be affected by the motions occurring in the amorphous regions. Hence, the more rapid decrease of $f(T)$ and A_c above T_g is most likely due to an increase of the internal disorder of the crystals, strains and paracrystalline disorder, with temperature. This is consistent with the conclusions drawn from the examination of the temperature variation of $\alpha_{v,c}$ in the previous paragraph.

The thermal expansion coefficient of the long period with temperature is 4.3 × 10^{-4} °C^{-1} above T_g. Since the crystal expansion along the c-axis is small,[36] this value is reasonable when compared to the volume thermal expansion coefficient of the amorphous regions ($\alpha_{v,a}$) which dominates the expansion of the stacks. However, the possible melting of thinner less stable lamellae lying between more stable ones must be considered, when analyzing the temperature variation of L. In this hypothesis, these lamellae would reappear upon cooling to give the observed reversible behavior. Suppose that all the variation of L with temperature is

due to such an effect. Then, the relative number of lamellae melting in the stacks would approximately equal the relative expansion of L. Thus, at most 4% of the lamellae in the stacks would melt per 100 °C elevation above T_g. The corresponding variation of linear crystallinity in the fibrils would obviously not be large enough to affect significantly Q or A_c. Taking now thermal expansion into account, we conclude that if there are any lamellae melting in the lamellar stacks in these experiments, their number must be extremely small and may be neglected.

In summary, all variations observed when heating well-crystallized samples below their crystallization temperature are reversible and only due to atomic vibrations, variations of the paracrystalline disorder of the crystals, and differences of thermal expansion between crystalline and amorphous regions. No melting or crystallization occurs in a sufficient amount to be detected. Thus, the set of curves in Figures 1 and 2 constitute the "zero base line" against which the occurrence of real morphological changes will be assessed in subsequent experiments. Throughout the remainder of this work, the term "reversible" will only be used to qualify phenomena identical to those described above.

B. Continuous Heating of Initially Amorphous Samples. In this section, we examine the changes occurring during the heating of amorphous samples. Since our experimental setup is restricted to temperatures below 300 °C, no data will be presented on the final melting of PEEK which occurs at higher temperatures. Below 300 °C, the DSC thermograms of the PEEK/PEI samples exhibit only a glass transition followed by a crystallization exotherm, whose locations depend on the PEI content.

The morphological data pertaining to the direct heating of amorphous PEEK and PEEK/PEI blends have been collected in Figures 3 and 4. In these figures, the thick solid line refers to the reversible behavior described in the previous section. Two successive regions can be distinguished in these data. In the first temperature range, the long period decreases with temperature, while at the same time the invariant and the apparent crystallinity increase rapidly. This corresponds to the crystallization region where ϕ_s increases; i.e., the spherulites grow in size and the spherulite volume is progressively filled by new lamellae. Apparently, the average distance between the crystals in the fibrils (L) decreases at the same time. Since the lamellar thickness remains constant in this stage, a corresponding increase of the linear crystallinity in the stacks is observed. Thus, during this primary stage, both ϕ_s and $\phi_{c,lin}$ increase significantly. It was unfortunately not possible to follow the very first evolution of the unit cell dimensions, as the crystalline reflections were too diffuse.

In the second region, crystallization is completed, and the structure evolves dynamically with temperature. For the pure PEEK sample, there are no amorphous regions in significant amounts outside the lamellar stacks ($\phi_s = 1$), as we have demonstrated quantitatively elsewhere.[6] This is not the case for the blends, where PEI tends to reside outside the lamellar stacks.[6] The long period and the average crystal thickness increase more rapidly than expected from reversible effects alone. At the same time, the apparent crystallinity remains constant. Given the decrease of A_c observed when only reversible effects are operative, the constancy of A_c actually corresponds to an increase of either the crystalline perfection or the linear crystallinity (eq 2). The invariant increases slightly more rapidly than can be accounted for by thermal expansion (this will be treated more fully later). Again, this may be due to an increase of the linear crystallinity in the fibrils or to an increase of the crystal density due to an improvement of the crystalline perfection. Since the ratio of L_c and L, i.e., $\phi_{c,lin}$, barely increases from 0.26 to 0.27 in this temperature range, it can be concluded that the effects observed on Q and A_c are mainly due to an improvement of the crystalline perfection. This is supported by the results on the change of the unit cell dimensions normal to the chain axis. The b-axis is independent of temperature which, when compared to the expected increase due to thermal expansion, corresponds to a densification of the packing in this direction. Less densification is observed along [100]. The results clearly demonstrate that the crystals perfect during heating.

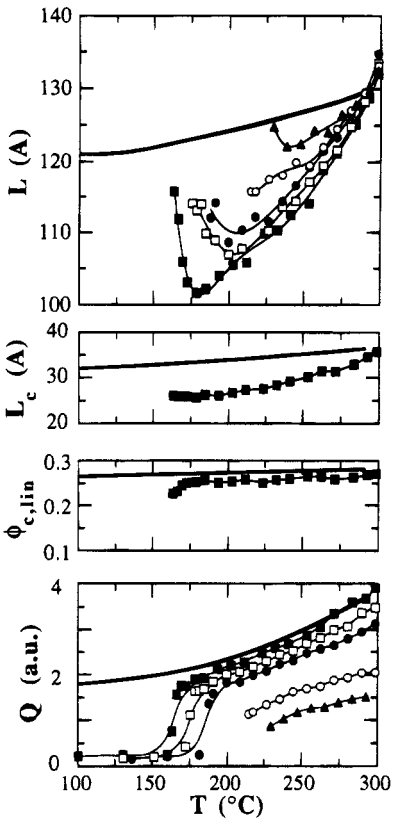

Figure 3. Evolution of the SAXS long period (L), the average lamellar thickness (L_c), the linear crystallinity ($\phi_{c,lin}$), and the SAXS invariant (Q), upon heating at 3 °C min^{-1} initially amorphous PEEK/PEI samples. The thick lines refer to the reversible variations observed when scanning well-crystallized PEEK samples below their last annealing temperatures. PEI weight contents: ■, 0%; □, 10%; ●, 20%; ○, 40%; ▲, 60%.

As can be seen, the observations made for pure PEEK are also valid for the blends. The dominant effect of the PEI is to retard the onset of crystallization. The magnitudes of the apparent crystallinity and invariant are reduced in proportion to the concentration of the crystallizable species. But the shape of the $Q(T)$ and $A_c(T)$ curves is preserved. The unit cell dimensions are independent of the PEI content, within experimental error. Except for temperatures near the T_g's of the blends where kinetic effects are prominent, the long period is governed mainly by the temperature and only slightly by the previous thermal history or PEI content. These experiments illustrate that, although the crystallization kinetics is strongly dependent on a transport

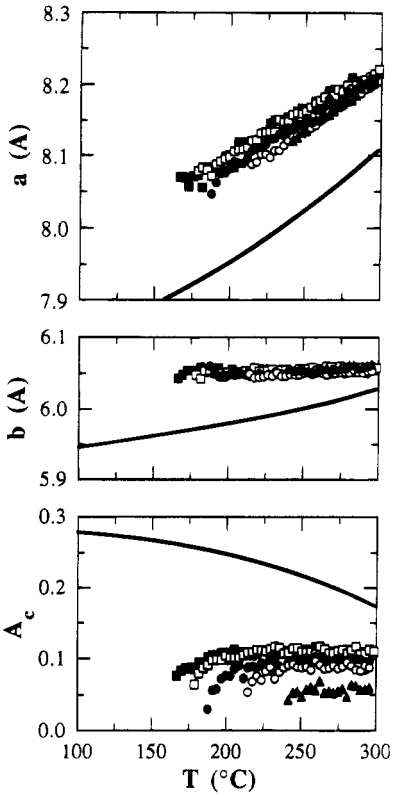

Figure 4. Evolution of the unit cell dimensions along [100] (a) and [010] (b), and of the apparent crystallinity (A_c, eq 2), upon heating at 3 °C min^{-1} initially amorphous PEEK/PEI samples. The thick lines refer to the reversible variations observed when scanning well-crystallized PEEK samples below their last annealing temperature. PEI contents: ■, 0%; □, 10%; ●, 20%; ○, 40%; ▲, 60%.

factor, the sample morphology is hardly affected by this term. This observation corresponds to the theoretical arguments where the morphology is dominated by thermodynamic factors, such as the critical thickness of a secondary nucleus in nuclation theories[40] or the energetic interactions between chain segments together with a set of pinning rules in entropy barrier theories.[41] The growth rate, on the other hand, depends on the transport factor.

C. Heating–Cooling Cycles. In order to attain a more precise description of the morphological changes occurring during heating, {heating; holding at T_c; cooling} cycles have been performed on initially amorphous samples, with increasing values for the annealing temperature T_c. In this way, it is easy to distinguish the variations due to reversible effects from those due to morphological changes, while removing any uncertainty arising from the use of different samples. This will also allow us to follow the changes occurring above T_c, which will provide insight into the origin of the double melting observed for cold-crystallized PEEK.

An amorphous sample of PEEK was heated at 3 °C min^{-1} to 160 °C, held 20 min at this temperature, and cooled to below T_g (100 °C) at −3 °C min^{-1}. The sample was then successively heated to T_c, held 10−15 min at T_c, and slowly cooled to below T_g (usually 100 °C), where T_c's of 200, 270, and 300 °C were used. Data were acquired throughout the thermal cycle.

Before detailing the scattering results, the heating DSC scans obtained during similar thermal cycles, shown in Figure 5, will be discussed. Since data pertaining to the isothermal annealing and cooling scans are not very illuminating, we will not discuss

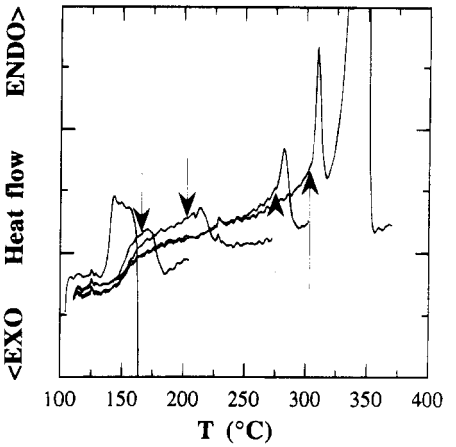

Figure 5. DSC heating thermograms (3 °C min^{-1}) of a PEEK sample successively annealed at higher temperatures (see text). First trace: initial amorphous sample; second trace: previous sample, annealed 20 min at 160 °C; third trace: previous sample, annealed 15 min at 200 °C; fourth trace: previous sample annealed 10 min at 270 °C; last trace: previous sample annealed 10 min at 300 °C. The arrow on each scan indicates the location of the last annealing temperature.

them here. In the first scan, the amorphous sample passes through its glass transition, then begins to crystallize just before the first holding temperature (the crystallization ends in the subsequent isothermal scan, not shown). The glass transition is still visible in the subsequent heating scans, though it occurs at higher temperatures in the semicrystallized polymer than in the amorphous one, as described in detail elsewhere.[42,43] In these scans, the calorimeter records a sudden relative release of energy each time the temperature goes beyond the last annealing temperature; this phenomenon is preceded by a small endotherm on the scans performed after annealing at the highest T_c's. A supplementary heating ramp has been finally performed to record the full melting of the sample, which occurs around 310–350 °C. This final melting endotherm would have been recorded for each scan, had we not stopped the heating scans at the selected T_c's. The double-melting behavior of cold-crystallized PEEK is clearly apparent in some of these scans.

It is interesting to examine the evolution of the dynamical modulus (E') of a sample subjected to a similar cycle, as shown in Figure 6. After a large drop in the T_g range, E' experiences a progressive decrease. When the temperature goes above the last T_c, the modulus decreases slightly more rapidly over a temperature range corresponding to the first melting endotherm detected by DSC. At higher temperatures, it superposes on the curve corresponding to a sample that was crystallized at a very low temperature. At this stage, the sample has thus lost all memory of its previous T_c. Upon annealing at a higher T_c, the modulus increases slowly with time. Cooling the sample to room temperature, then reheating it to T_c, brings the modulus back to the last value previously reached at T_c. Consequently, the process is reversible. Irreversible changes in the modulus occur only by holding the sample at T_c for longer times, or by passing over T_c.

Typical X-ray scattering curves corresponding to such cycles are shown in Figures 7 and 8. The evolution of the long period L during a series of thermal cycles is shown in Figure 9, which will be discussed in detail since the remaining figures are formally identical to this one. The evolution of L with time is represented on the

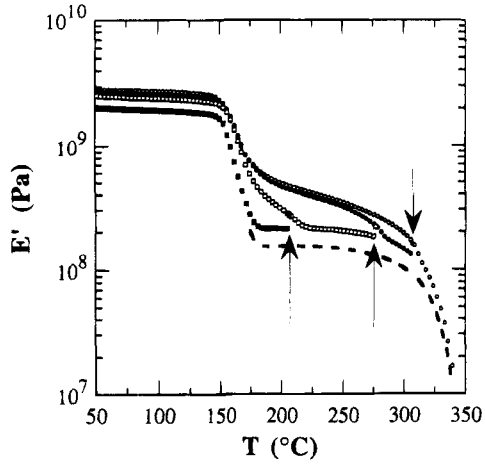

Figure 6. Dynamic elastic modulus of a PEEK sample successively annealed at higher temperatures (1 Hz; 3 °C min^{-1}). ■, amorphous glassy sample annealed 20 min at 160 °C; □, previous sample annealed 15 min at 200 °C; ●, previous sample annealed 10 min at 270 °C; ○, previous sample annealed 10 min at 300 °C. The arrows indicate the locations of the annealing temperatures. The values of the modulus after the annealing at each T_c are also indicated on this figure. The dashed line represents the evolution of E' with temperature for a sample annealed 20 min at 160 °C upon direct heating (shifted downward for clarity). No scans were performed on the initial fully amorphous sample, because creeping in the glass transition region was too large for such a sample.

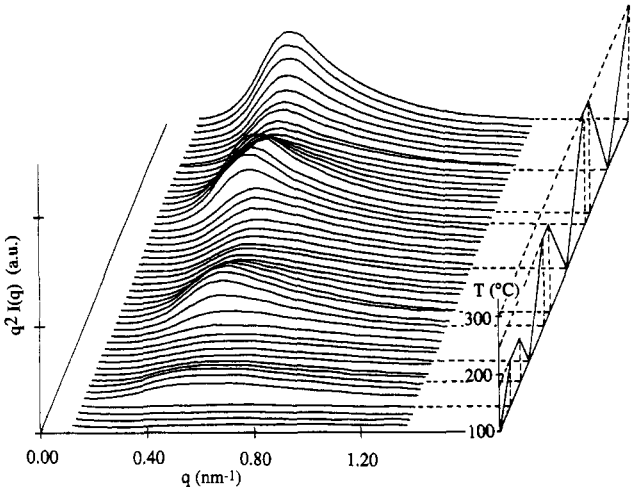

Figure 7. Typical Lorentz-corrected SAXS patterns of an initially amorphous PEEK/PEI sample (20% PEI) successively heated at 3 °C min^{-1} to increasingly higher temperatures and cooled to below T_g between each heating scan. Although data have been acquired every minute along the thermal cycle, only one curve every 9 min is displayed here for clarity. Similar experiments have been performed on PEEK, PEEK/PEI 40/60, and PET.[2]

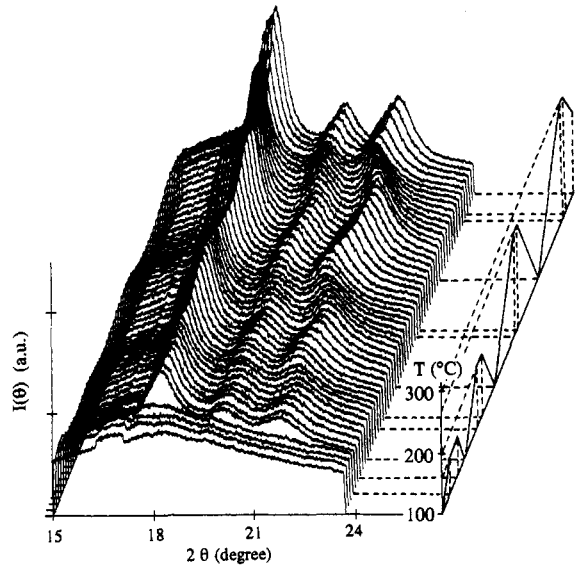

Figure 8. Typical WAXS patterns of an initially amorphous PEEK sample successively heated at 3 °C min^{-1} to increasingly higher temperatures and cooled to below T_g between each heating scan. Although data have been acquired every minute along the thermal cycle, only one curve every 9 min is displayed here for clarity. Similar experiments have been performed on PEEK/PEI 80/20 and PEEK/PEI 40/60. The step around 17° in the curves corresponds to a slightly damaged section of the detector (appropriate corrections were performed before computing parameters from these curves).

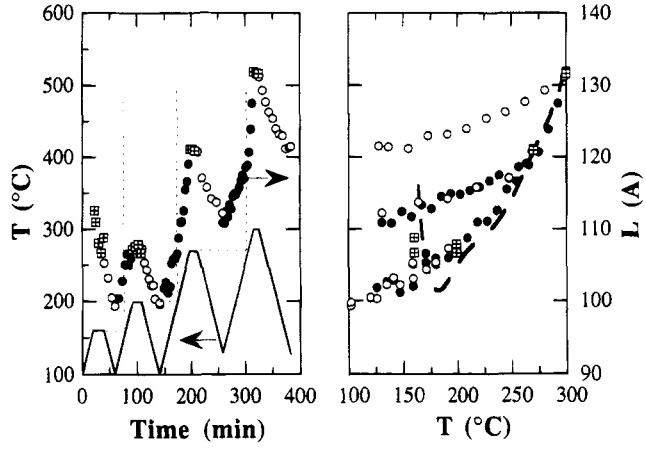

Figure 9. Left: Time evolution of the temperature (continuous line) and of the SAXS long period of a PEEK sample subjected to heating–annealing–cooling cycles with increasing annealing temperatures. Right: The same data, plotted as a function of temperature (some of the points pertaining to the first annealing have been removed for clarity). The dashed line represents the evolution of L with temperature for an initially amorphous sample directly heated in the beam at 3 °C min^{-1} to 300 °C. Symbols: Filled symbols refer to heating sections, open ones to cooling sections, and crossed squares to annealing sections.

left-hand side of Figure 9. L is indicated by circles and squares, whereas the temperature cycling is shown by the solid line. In this and the following graphs, filled circles always refer to heating ramps, open circles to cooling ramps, and crossed squares to isotherms. The long period first decreases during the initial crystallization, which occurs mainly isothermally at 160 °C. Then, upon successive cooling and heating runs, L decreases and increases regularly. No significant changes can be observed in L when the temperature is held constant. The right-hand side of Figure 9 shows the same data as a function of temperature. For clarity, we have removed most of the points corresponding to the first isotherm, i.e., the crystallization from the amorphous glass where L decreases. This representation is very informative because it allows one to readily separate reversible effects from actual morphological changes. The figure can be described as being made of an irreversible branch onto which are grafted less sloped reversible branches, associated with each T_c. For each of the annealing temperatures, the temperature dependence of the data on the associated reversible branches is identical, with the variations in L being due to thermal expansion and other reversible phenomena. Departure from this reversible behavior occurs when the sample is brought above T_c, at which point the change in L with temperature increases. Once T_c is exceeded,

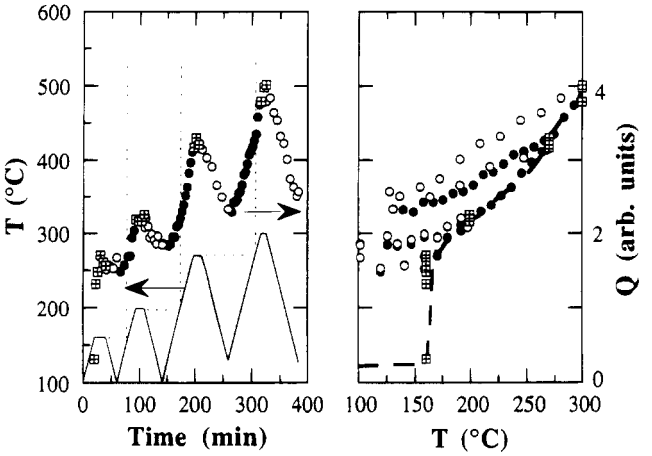

Figure 10. Left: Time evolution of the temperature (continuous line) and of the SAXS invariant of a PEEK sample subjected to heating–annealing–cooling cycles with increasing annealing temperatures. Right: The same data, plotted as a function of temperature. The dashed line represents the evolution of Q with temperature for an initially amorphous sample directly heated in the beam to 300 °C. Symbols: Filled symbols refer to heating sections, open ones to cooling sections, and crossed squares to annealing sections.

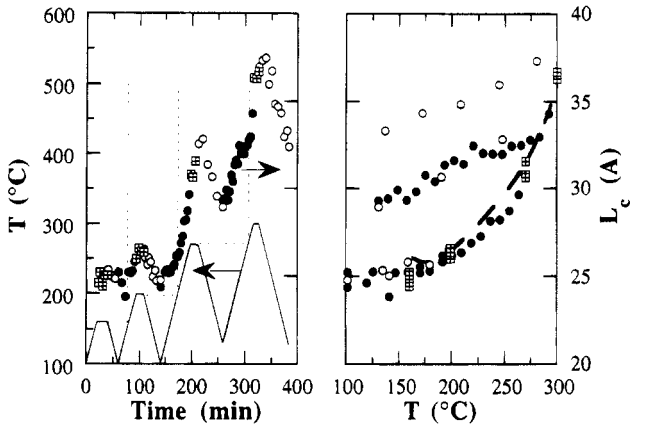

Figure 11. Left: Time evolution of the temperature (continuous line) and of the average crystal thickness of a PEEK sample subjected to heating–annealing–cooling cycles with increasing annealing temperatures. Right: The same data, plotted as a function of temperature. The dashed line represents the evolution of L_c with temperature for an initially amorphous sample directly heated in the beam to 300 °C. Symbols: Filled symbols refer to heating sections, open ones to cooling sections, and crossed squares to annealing sections.

the changes are irreversible, and real morphological changes occur. For the lowest annealing temperatures, the distinction between irreversible and reversible branches is not obvious, as the variations of L are small when compared to the precision of the measurements. The temperature dependence of L, obtained by heating an amorphous sample, is also shown in the figure as the dashed line. It is obvious that these data and the irreversible branch are virtually identical.

Similar plots for the invariant (Q), the average lamellar thickness (L_c), the average thickness of the noncrystalline layers (L_a), the linear crystallinity ($\phi_{c,lin}$), the unit cell dimensions, and the apparent crystallinity (A_c) are shown in Figures 10–16. For each quantity, reversible and irreversible branches are seen, the irreversible branch coinciding with the curves obtained by heating an amorphous sample in the beam, the reversible ones being parallel to the curves describing the effects of thermal expansion measured previously

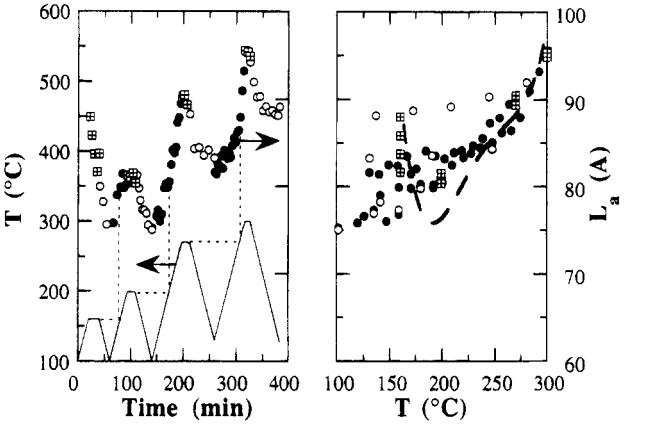

Figure 12. Left: Time evolution of the temperature (continuous line) and of the average amorphous interlayer thickness of a PEEK sample subjected to heating–annealing–cooling cycles with increasing annealing temperatures. Right: The same data, plotted as a function of temperature. The dashed line represents the evolution of L_a with temperature for an initially amorphous sample directly heated in the beam to 300 °C. Symbols: Filled symbols refer to heating sections, open ones to cooling sections, and crossed squares to annealing sections.

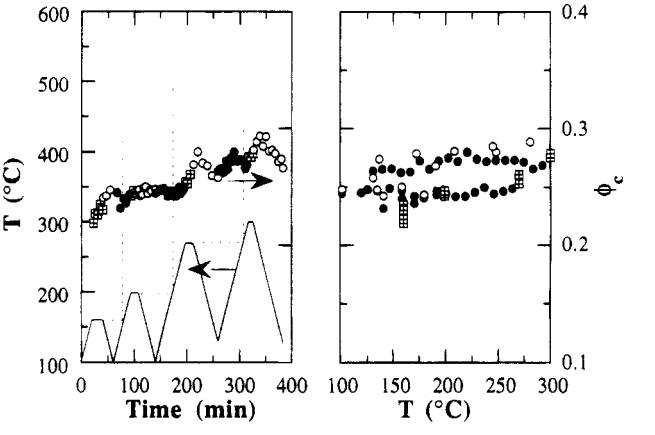

Figure 13. Left: Time evolution of the temperature (continuous line) and of the linear crystallinity of a PEEK sample subjected to heating–annealing–cooling cycles with increasing annealing temperatures. Right: The same data, plotted as a function of temperature. Symbols: Filled symbols refer to heating sections, open ones to cooling sections, and crossed squares to annealing sections.

on well-crystallized samples. The following observations can be made:

(1) Below the last annealing temperature T_c, all structural parameters are reversible up to T_c. The location of this reversible branch is determined mainly by T_c, and to a lesser extent by the annealing time at T_c.

(2) During annealing at T_c, a densification of the crystals along the a-axis and an increase of the apparent crystallinity and of the sample elastic modulus occur. An increase of L_c can also be detected, while the other structural parameters are not significantly affected.

(3) As soon as temperature goes beyond the last T_c, structural changes occur immediately. When compared to the reversible behavior, these changes are characterized by an irreversible increase of the long period, of the apparent crystallinity, of the invariant, of the average thickness of the lamellae and interlamellar noncrystalline regions, and of the crystal density. However, the linear crystallinity is not significantly affected, since the changes in L_c and L essentially cancel

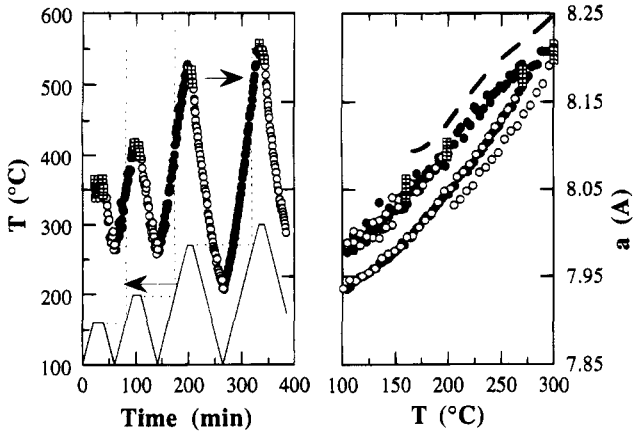

Figure 14. Left: Time evolution of the temperature (continuous line) and of the unit cell dimension along [100] of a PEEK sample subjected to heating–annealing–cooling cycles with increasing annealing temperatures. Right: The same data, plotted as a function of temperature. The dashed line represents the evolution of a with temperature for an initially amorphous sample directly heated in the beam to 300 °C. Because this line is virtually indistinguishable from the irreversible branch (see text), it has been displaced upward by 0.03 Å. Symbols: Filled symbols refer to heating sections, open ones to cooling sections, and crossed squares to annealing sections.

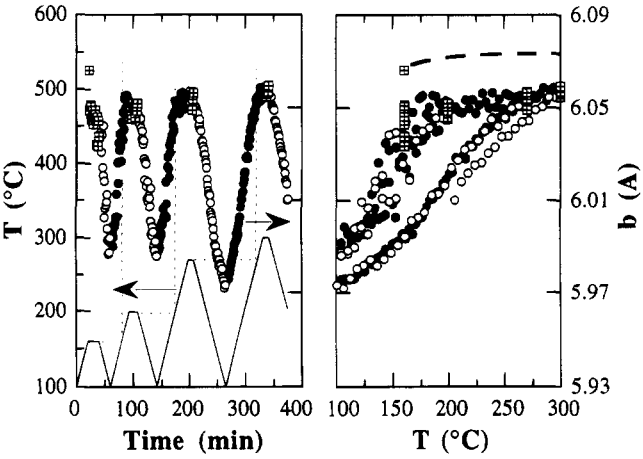

Figure 15. Left: Time evolution of the temperature (continuous line) and of the unit cell dimension along [010] of a PEEK sample subjected to heating–annealing–cooling cycles with increasing annealing temperatures. Right: The same data, plotted as a function of temperature. The dashed line represents the evolution of b with temperature for an initially amorphous sample directly heated in the beam to 300 °C. Because this line is virtually indistinguishable from the irreversible branch (see text), it has been displaced upward by 0.02 Å. Symbols: Filled symbols refer to heating sections, open ones to cooling sections, and crossed squares to annealing sections.

each other. As shown by the DSC results, a release of energy occurs with these changes and is preceded sometimes by a sharp energy absorption. The morphological changes occur rapidly during the heating scans. The structural changes are such that the morphology obtained at a given temperature above T_c is the same as that obtained by directly heating the sample to this temperature, irrespective of the previous thermal history. The structure has no memory of events which have occurred at lower temperatures.

Before discussing these results, we would like to emphasize that the above-described behavior is not limited to pure PEEK. Similar WAXS and SAXS real-time experiments have been performed on some PEEK/PEI blends and give exactly the same results, except of course for an expected temperature shift. Cyclic SAXS experiments have also been performed on PET.[2] Below 215 °C, the SAXS observations are similar to those described in the present paper.

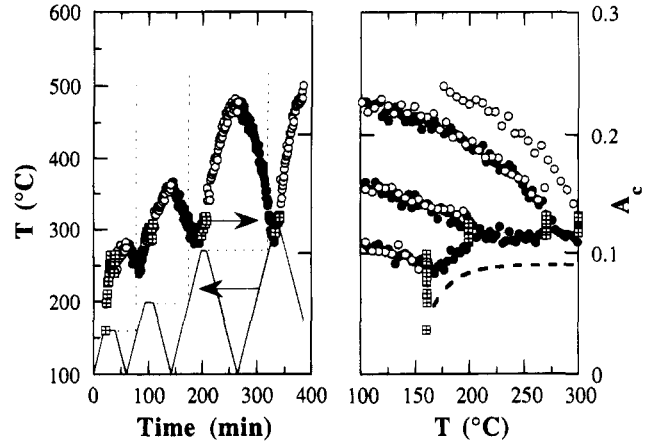

Figure 16. Left: Time evolution of the temperature (continuous line) and of the apparent crystallinity of a PEEK sample subjected to heating–annealing–cooling cycles with increasing annealing temperatures. Right: The same data, plotted as a function of temperature. The dashed line represents the evolution of A_c with temperature for an initially amorphous sample directly heated in the beam to 300 °C. Because this line is virtually indistinguishable from the irreversible branch (see text), it has been displaced downward by 0.02. Symbols: Filled symbols refer to heating sections, open ones to cooling sections, and crossed squares to annealing sections.

Discussion

A. The Crystallization Region. The data acquired in this work in the crystallization region are similar to those reported previously for the isothermal crystallization of aromatic polymers.[16–20] During this stage, both the invariant and the apparent crystallinity increase over time, reflecting the overall increase of the crystallinity of the sample. The simultaneous decrease of the long period has been previously interpreted as arising from the progressive insertion of new lamellae in-between existing ones. Recent simulations[44] of the SAXS signal from lamellar stacks of finite size reveal that a decrease of the long period also results from an increase of the average number of lamellae per stack (N). A similar behavior is also observed for the location of the first maximum of the one-dimensional correlation function. This effect, arising from incomplete extinction and the form factor of the lamellar stack, is significant only for N smaller than ~5 lamellae per stack and may also account for part of the decrease of L over time during the primary crystallization. For PEEK/PEI blends, one expects that the occurrence of lamellae insertion be reduced as compared to pure PEEK, since lamellae in these blends tend to grow in tightly packed lamellar bundles, isolated from each other by large amounts of pure PEI.[6] This probably explains the smaller decrease of L over time observed for the PEI-rich blends.

Most significant is the fact that the estimated crystal thickness remains approximately constant during crystallization. Since L_c reaches a constant value before Q reaches 50% of its value at the end of the primary crystallization (Figure 3), it follows that much more than half of the crystallized material is made of lamellae of equal thickness at the end of the crystallization process. Moreover, an examination of the data of Hsiao

et al.[19,20] reveals that L_c is also constant from times at which the invariant has not yet reached 20% of its final value, when PEEK is crystallized isothermally from the melt at temperatures between 230 and 300 °C. This demonstrates that most of the lamellae have the same average thickness at the end of the crystallization process, unless some of them do not contribute to the SAXS signal in the probed angular range. This exception can be ruled out, since we have shown elsewhere[6] that the intensity of the SAXS signal at the end of the crystallization is in quantitative agreement with the crystalline content measured independently by an absolute method.

Thus, the results shown here support the predominance of a single lamellar population of nearly uniform thickness, as expected from crystallization theories of homogeneous polymers.[41] The existence of some *thicker* lamellae cannot be ruled out completely, but these have to account for *much less* than 20% of the total. It is important to note that a SAXS maximum is usually detected before any distinct crystal reflections are seen with WAXS. This confirms that, as noted by others,[45] SAXS is a more sensitive technique than WAXS to detect the onset of crystallization. Unfortunately, this prevents one from obtaining more information on the initial stages of the crystallization by WAXS.

B. Irreversible Behavior: A Melting–Recrystallization Mechanism. The results indicate that the structure of aromatic polymers crystallized from the glassy state is stable below the last annealing temperature T_c, while it never ceases to evolve above T_c, at least for T_c's higher than T_g + ~30–40 °C. Upon heating a sample beyond T_c, the following happens:

1. L, L_a, and L_c Increase Irreversibly with T. These observations are not compatible with a process wherein only a few (slightly) thinner lamellae would melt randomly in the lamellar stacks. Indeed, in such a case, the melting lamellae would not recrystallize, since L increases. Moreover, the irreversibility of this increase would imply that a rapid thickening of the neighboring lamellae occurs, preventing an interlamellar recrystallization upon cooling. But such a thickening mechanism can be safely ruled out, since it should also have been operative during the primary crystallization, contrary to the experimental observations.

Thus, we conclude that *at least* some whole stacks of slightly lower L and L_c must be melting in the sample. Since the effects observed are irreversible, melting must be directly followed by another structural modification such as crystallization. Otherwise, the molten material would recrystallize upon cooling, which is inconsistent with the observation of an irreversible behavior. Therefore, the melting of a stack must be followed immediately by its recrystallization in a new stack of larger L and L_c. This confirms the existence of a melting–recrystallization mechanism occurring above the last T_c, which concerns whole stacks. Given the existence of a single lamellar population essentially, the melting–recrystallization occurs throughout the entire sample, with slight local variations of its onset that reflect the local distribution of lamellar thickness.

2. The Density of the Crystals Increases. This is a direct consequence of the increase of the average crystal thickness due to recrystallization. Strains induced in the crystals by the connection of the crystalline stems to the noncrystalline regions are reduced on the average, thereby allowing a denser packing. An intriguing observation is that the value of b remains constant during the whole melting–recrystallization process (Figures 4 and 15). The interchain distance along b never increases beyond about 6.05 Å.

3. The Linear Crystallinity in the Samples Increases Only Slightly. Although the uncertainty of the data analysis, due among other things to the neglect of the existence of density transition layers, is too large to detect small variations of linear crystallinity, it is clear that, far away from the final melting point, L and L_c increase similarly, holding an approximate proportionality among themselves. Since $\phi_s = 1$ in the samples crystallized to completion, the overall actual crystallinity of the samples should also depend only slightly on T_c. This is precisely what has been observed at room temperature on samples crystallized from the glass and rapidly cooled to room temperature,[6] where it was found that the bulk crystallinity increased little for T_c's between 160 and 300 °C (the comparison is valid, since we have demonstrated that no morphological changes occur when cooling the polymers from their last annealing temperatures to room temperature, at least for cooling rates faster than 3 °C min^{-1}).

4. The Apparent Crystallinity A_c, and the Invariant, Increase Significantly. Even though the linear crystallinity of PEEK increases only slightly below 300 °C, the apparent bulk crystallinity increases strongly above the last T_c when compared to its reversible behavior. This observation parallels the densification of the crystals already noted: the irreversible changes in A_c are largely due to a decrease in the internal disorder of the crystals, due to a better repartitioning of the stresses in the crystals generated by the tethering of the chains to the noncrystalline regions. Similarly, the irreversible increase of the invariant results largely from the increased crystal density which accompanies the overall lamellar thickening (eq 1). Small variations of $\phi_{c,lin}$ account for the rest of the variation of these two parameters.

In conclusion, the experimental results show that the sample is essentially made of stacks of lamellae having almost all the same thickness; that these stacks undertake a melting–recrystallization as soon as temperature goes beyond the last highest annealing temperature; and that the new structure formed is characterized by thicker and more perfect lamellae, with only small changes in the total crystal content. We emphasize that the effects detected on the structural parameters result largely from lamellar perfection, at least for temperatures ~40 °C below the final melting. This clearly bears important practical consequences with respect to the interpretation of scattering data, a frequently overlooked fact.

The mechanism just described explains the observation that the sample has no memory of events having occurred below its last highest annealing temperature, since any morphological detail due to such an event is erased irreversibly by the melting–recrystallization mechanism. It also explains the downward jump observed in the DSC trace just above the last annealing temperature (Figure 5). Above T_c, the interchain distance decreases as compared to what would have been measured under reversible conditions (Figures 14 and 15). Consequently, the internal energy of the crystals increases less rapidly with temperature than in reversible conditions, due to the extra interchain energy provided by the continuous densification of the crystals. Therefore, the energy required to heat the sample at a constant rate decreases, which manifests itself in a

downward jump in the DSC trace. The endothermic peak appearing just above the last annealing temperature can be attributed to the initiation of the melting process. Given the limited time resolution of the present study, it is not surprising that no clear effect can be observed on our experimental curves during the short time in which more material is melting than recrystallizing. The final melting peak corresponds to the melting of the extensively perfected crystals.

C. Annealing and Its Influence on the Low Temperature Melting Endotherm. Recently, on the basis of SAXS measurements, it has been claimed[25] that no morphological changes are associated with the development of the low melting temperature endotherm over annealing time. This claim, together with the fact that the kinetics of this development resembles that of an enthalpic relaxation type process, led Velikov *et al.*[46] to ascribe the low melting endotherm to an ill-defined relaxation process occurring in the amorphous regions. However, the results of the present study clearly demonstrate that thickening and perfecting of lamellae occur during annealing, as indicated by the increasing crystal density and lamellar thickness. Accordingly, as a consequence of these variations in the quality of the crystalline regions, the elastic modulus of the sample increases over annealing time.

D. Comparison between Samples Crystallized from the Glass and from the Melt. There is a clear resemblance between the experimental results of Hsiao *et al.*[19,20,22] obtained on PEEK *isothermally crystallized from the melt* (T_c = 230–300 °C) and our own results obtained on PEEK annealed from the glass. For instance, for Hsiao *et al.*'s samples, the rate of increase of the long period with temperature is small below the previous crystallization temperature and more rapid above it, exactly as we found for cold-crystallized samples (compare Figure 10 of ref 22 with Figure 9 of the present paper). Therefore, it seems likely that the melting–recrystallization mechanism described in the present paper applies to samples isothermally crystallized from the melt as well. It is more difficult to compare our results with results obtained on samples isothermally crystallized from the melt at high temperature[25] above 300 °C, as the temperature ranges do not overlap. Moreover, as described in the Introduction, many uncertainties are still confusing the interpretation of the double-melting behavior of such high temperature-crystallized samples. A comparison is thus probably inappropriate at the present time.

In the Introduction, mention was made of results[23] that assign the multiple melting behavior of PEEK *crystallized stepwise from the melt* to the presence of lamellar populations of different thicknesses. These results are not inconsistent with our findings. When crystallizing PEEK from the melt at high temperatures, segregation effects could interfere with the crystallization, given the slow crystallization kinetics and relatively large molecular mobility. We have shown elsewhere[47] that the commercial polymer contains a few percents by weight of low molecular weight species. Moreover, it has been shown[28,29] that improper processing induces branching of PEEK, with a subsequent slowing down of the crystallization kinetics. At this stage, we recall that poly(ether imide), a polymer compatible with PEEK in the amorphous state, is mostly expelled from the crystalline stacks of PEEK to the interfibrillar regions. This suggests that less-crystallizable defects of pure PEEK will also tend to be expelled to the region between PEEK crystalline fibrils. Upon step cooling, these impurities will progressively crystallize, giving rise to the observed multiple melting. This does not occur in cold-crystallized samples, because they are crystallized at very high supercoolings where segregation effects should be minimal.

E. The Crystal Thickness Limitations. As explained in the Experimental Section, the determination of L_c is subject to some uncertainty. This uncertainty results from the Babinet's reciprocity theorem,[48] which states that light is diffracted by a white-on-black pattern in the same way as by the reverse black-on-white pattern. Thus, it is impossible to decide *a priori* whether the thickness we have assigned in this study to the crystals should not actually be assigned to the interlamellar amorphous regions. More precisely, from the analysis of the correlation function, we obtain two lengths, L_m and L_M, whose sum equals the average center to center distance of the crystals (i.e., the long period L). Let us fix $L_m < L_M$. In the present study, we have assigned the crystal thickness to the shorter length (L_m), and the amorphous interlayer to the larger one (L_M). Recently, other authors have claimed that the reverse selection should be made.[5,20,22,25] This bears important consequences, as part of our interpretation would have to be revised. In this section, we will thus provide justifications for our choice and arguments against the reverse case.

Arguments in favor of the reverse picture are as follows:

(i) If L_m is considered to be the crystal thickness, the computed linear crystallinity ($\phi_{c,lin}$) is sometimes found to be smaller than the bulk crystallinity. However, this is the case only when bulk crystallinities are estimated by methods known to lead only to approximate values for the crystallinity.[5,20,22] We have shown elsewhere[6] that there is no discrepancy when the bulk crystallinity is computed by an absolute method like Ruland's method. Note also that estimates of the crystallinity by density would suffer from the same shortcoming, if the variation of the crystal density with lamellar thickness is not taken into account. Estimation by calorimetric methods will also be somewhat questionable.[49]

(ii) PEEK lamellar thicknesses around 150 Å have been measured by electron microscopy,[26] in close proximity to the values of the long period. These results were obtained on samples that have been crystallized in thin films, usually at very low supercoolings (~320 °C). This is undoubtedly a situation relatively remote from the bulk samples studied by X-ray scattering. Moreover, the substrates selected to cast the PEEK films (freshly cleaved mica) promote a significant "edge-on" orientation of the lamellae during crystallization, which has been attributed to an interaction between the mica and the PEEK chains.[50] The way this interaction affects the observed lamellar thicknesses is however unknown.

Having given the arguments in favor of the "reverse" picture, and the elements that lead us to consider them at best questionable, we present some arguments that, in our view, definitively support the assignment of L_m to L_c.

(i) A study of the properties of PEEK/PEI blends[6] has shown that, at constant annealing temperature and upon increasing PEI content, L_M increases slightly, while L_m remains constant. Given the very small melting point depression of PEEK/PEI blends, it is clear that the lamellar thickness is expected to remain

constant. The amorphous interlayer, on the contrary, may increase due to the limited presence of PEI in-between the PEEK lamellae. The limited presence of PEI in the interlamellar regions was corroborated by a dielectric relaxation study.[6] Therefore, it is appropriate to assign L_m to L_c, and the larger L_M to the amorphous interlayer.

(ii) It has been shown elsewhere[43] that an analysis of the SAXS data by the correlation function approach (with $L_c = L_m$) gives results in good agreement with the very simple evaluation of the lamellar thickness obtained by multiplying the long period by the bulk crystallinity, *for a very wide range of samples*. Although some reservations can be made on the accuracy of the crystallinity determinations, the general pattern is clear and suggests that the linear crystallinity should not be very different from the bulk crystallinity, which is only true if $L_c = L_m$. Moreover, a recent quantitative study[6] also shows that the absolute value of the SAXS invariant is consistent with data coming from WAXS and density determinations, when L_c is equated to L_m.

(iii) The very low values of the structure factor of the (001) reflections of PEEK prevent one from obtaining the crystal thickness from a broadening analysis of these reflections, for *isotropic* PEEK. An estimation of the crystal thickness from a broadening analysis of other reflections is also very difficult, because the microfragmentation of PEEK lamellae[50] significantly restricts the size of the coherently diffracting domains in the directions perpendicular to the chain axis as well. However, Yoda[51] succeeded in performing a line broadening analysis on a succession of (001) reflections for *drawn* PEEK crystallized at 300 °C; the effects of both paracrystalline distortions and crystallite size were taken into account. The results give 0.4 as linear crystallinity, which is more consistent with the ~0.3 found for isotropic PEEK by the SAXS analysis than with the ~0.7 advocated by the proponents of the reverse picture. At this stage, it is appropriate to comment on the limited accuracy of our simple analysis of the correlation function. As shown elsewhere,[6] this analysis tends to slightly underestimate $\phi_{c,lin}$. Moreover, the ideal lamellar model used to represent the data is but an approximation of a much more complex reality (curved or bent lamellae, wide and possibly asymmetric distributions of thicknesses, nonparallel lamellae, etc.). Its main advantage is that it allows one to process reasonably rapidly large amounts of data, in order to represent in a schematic way the trends of the data. However, one should exercise some caution when considering the absolute values of some of the parameters extracted from this analysis (especially $\phi_{c,lin}$ and L_c).

(iv) If the reverse picture were true, more than 50% of the polymer would be lying uncrystallized outside lamellar stacks (interfibrillar amorphous polymer). Indeed, since the figures given by Hsiao *et al.*[5] are about 0.3 for the bulk crystallinity and 0.75 for the linear crystallinity, it follows that ϕ_s is smaller than 0.5 (eq 2). Moreover, these interfibrillar regions do not contribute to the SAXS signal in the probed range; indeed, the addition of PEI, which is fully miscible with amorphous PEEK and is mainly rejected to the interfibrillar regions in the semicrystalline blends[4-6] (and, for the highest PEI contents, to the interspherulitic regions as well), decreases the invariant almost in linear proportion to the added amount of PEI (Figure 3). This proves that no signal due to the interference between the radiation scattered from neighboring stacks is present in the experimental SAXS range. Therefore, the size of the amorphous interfibrillar regions must be several hundreds of angstroms. Hence, the reverse picture requires the existence of large amorphous regions covering more than half the volume of the sample. This is clearly unreasonable, as no other experimental technique provides an indication for such large structural inhomogeneities, for samples similar to the ones of the present study.

From the previous discussion, it seems highly unlikely that the reverse picture is correct. Not only can the arguments of its proponents be discarded for one reason or another; moreover, several items of quantitative evidence are clearly in disagreement with this picture.

Conclusions

The following results have been established in the present work:

(1) Similarly to other aromatic semicrystalline polymers, PEEK crystallizes from the glass by a mechanism in which new lamellae progressively fill the free space left between already formed lamellae. This insertion mechanism occurs without significant variation of the thickness of the lamellae, and a single lamellar population is created. The insertion stops when topological constraints in the interlamellar amorphous regions (entanglements, etc.) prevent the growth of new lamellae.

(2) When crystallized or annealed at T_c from the glassy state, these polymers show no morphological variations below T_c, at least for cooling rates faster than 3 °C min^{-1}. Consequently, valid conclusions concerning the structure of such samples as a function of T_c can be drawn from investigations performed at room temperature only.

(3) Above T_c, a rapid, continuous melting–recrystallization of the lamellae occurs throughout the whole sample. Thus, any experimental technique where the sample is heated in order to get structural information should be considered with caution above T_c. The double-melting behavior of cold-crystallized PEEK and similar aromatic polymers is due to this mechanism, and not to the existence of different lamellar populations of varying crystallite thickness.

(4) The melting–recrystallization mechanism does not markedly increase the crystallinity of the samples. However, the lamellar thickness and perfection are significantly increased. As lamellae thicken, the constraints generated by the coupling of the stems to the amorphous regions are distributed over a larger volume, with a resulting denser chain packing in the crystals.

(5) During annealing at a temperature T_c, the crystals perfect and thicken slowly. This results in parallel variations of the elastic modulus, and in modifications of the low melting endotherm that signal the onset of the melting–recrystallization mechanism.

(6) The strong influence of the coupling between the lamellae and the noncrystalline regions has been pointed out more than once. The thermal expansion of the crystal, the crystal disorder, and the volume of the unit cell are all affected by this coupling. Clearly, the structure of the noncrystalline regions is a key parameter controlling the properties of the lamellae. Even the insertion mechanism of the lamellae is probably controlled by the building of topological constraints in the noncrystalline regions. Hence, it seems of prime importance to characterize the conformations of the chains in these regions, and the exact nature of the topological

constraints, before working out a quantitative theory of the crystallization and semicrystalline morphology of aromatic polymers. A more practical conclusion is that, because of this coupling, the variations of the SAXS invariant and of the WAXS apparent crystallinity must be interpreted with caution. Therefore, it is not appropriate, at least in the case of PEEK, to relate any increase of Q or A_c to a real increase of the volume fraction of crystalline material in the sample, because important variations of crystalline density and disorder may arise due to the redistribution of strains generated in the crystals by their connection to the noncrystalline regions.

Acknowledgment. The authors are indebted to Mrs. H. Truong for having performed the DSC experiments. A.M.J. wishes to express his gratitude to IBM Belgium for its financial support of this work, to NATO for a research fellowship, and to the U.S. Government for the award of a Fulbright-Hays research scholar grant-in-aid. T.P.R. acknowledges the partial support of the U.S. Department of Energy, Office of Basic Energy Sciences, under Contract FG03 88ER 45375.

References and Notes

(1) Nomenclature: PEEK stands for poly(oxy-1,4-phenyleneoxy-1,4-phenylenecarbonyl-1,4-phenylene); PEI stands for poly-{2,2'-(1,4-phenylenediimino)bis[(3,4-dicarboxyphenoxy)phenyl)-propane]}; PET stands for poly(oxyethyleneoxyterephthaloyl).
(2) Jonas, A. M.; Russell, T. P.; Yoon, D. Y. *Colloid Polym. Sci.* **1994**, *272*, 1344.
(3) Harris, J. E.; Robeson, L. M. *J. Appl. Polym. Sci.* **1988**, *35*, 1877. Crevecoeur, G.; Groeninckx, G. *Macromolecules* **1991**, *24*, 1190. Chen, H.-L.; Porter, R. S. *Polym. Eng. Sci.* **1992**, *32*, 1870.
(4) Hudson, S. D.; Davis, D. D.; Lovinger, A. J. *Macromolecules* **1992**, *25*, 1759.
(5) Hsiao, B. S.; Sauer, B. B. *J. Polym. Sci., Polym. Phys. Ed.* **1993**, *31*, 901.
(6) Jonas, A. M.; Russell, T. P.; Yoon, D. Y., submitted.
(7) For partial reviews on PEEK, see: Nguyen, H. X.; Ishida, H. *Polym. Compos.* **1987**, *8*, 57. Mullins, M. J.; Woo, E. P. *J. Macromol. Sci., Rev. Macromol. Chem. Phys.* **1987**, *C27*, 313. Jonas, A.; Legras, R. In *Crystallization of Polymers*; Dosière, M., Ed.; NATO ASI Series C, Vol. 405; Kluwer: Dordrecht and Boston, 1993; p 619.
(8) Cheng, S. Z. D.; Cao, M. Y.; Wunderlich, B. *Macromolecules* **1986**, *19*, 1868.
(9) Cebe, P.; Hong, S.-D. *Polymer* **1986**, *27*, 1183.
(10) Blundell, D. J. *Polymer* **1987**, *28*, 2248.
(11) Lee, Y.; Porter, R. S. *Macromolecules* **1987**, *20*, 1336.
(12) Bassett, D. C.; Olley, R. H.; Raheil, I. A. M. *Polymer* **1988**, *29*, 1745.
(13) Chang, S.-S. *Polym. Commun.* **1988**, *29*, 138.
(14) Lee, Y.; Porter, R. S.; Lin, J. S. *Macromolecules* **1989**, *22*, 1756.
(15) Lattimer, M. P.; Hobbs, J. K.; Hill, M. J.; Barham, P. J. *Polymer* **1992**, *33*, 3971.
(16) Elsner, G.; Koch, M. H. J.; Bordas, J.; Zachmann, H. G. *Makromol. Chem.* **1981**, *182*, 1263.
(17) Zachmann, H. G.; Wutz, C. In *Crystallization of Polymers*; Dosière, M., Ed.; NATO ASI Series C, Vol. 405; Kluwer: Dordrecht and Boston, 1993; p 403.
(18) Wang, J.; Alvarez, M.; Zhang, W.; Wu, Z.; Li, Y.; Chu, B. *Macromolecules* **1992**, *25*, 6943.
(19) Hsiao, B. S.; Gardner, K. H.; Wu, D. A.; Chu, B. *Polymer* **1993**, *34*, 3986.
(20) Hsiao, B. S.; Gardner, K. H. In *Crystallization of Polymers*; Dosière, M., Ed.; NATO ASI Series C, Vol. 405; Kluwer: Dordrecht and Boston, 1993; p 415.
(21) Elsner, G.; Zachmann, H.; Milch, J. R. *Makromol. Chem.* **1981**, *182*, 657.
(22) Hsiao, B. S.; Gardner, K. H.; Wu, D. A.; Chu, B. *Polymer* **1993**, *34*, 3996.
(23) Krüger, K.-N.; Zachmann, H. G. *Macromolecules* **1993**, *26*, 5202.
(24) Strobl, G. R.; Schneider, M. J.; Voigt-Martin, I. G. *J. Polym. Sci., Polym. Phys. Ed.* **1980**, *18*, 1361.
(25) Verma, R. K.; Kander, R. G.; Velikov, V.; Marand, H.; Hsiao, B.; Chu, B. *Bull. Am. Phys. Soc.* **1994**, *39*, 109. Verma, R. K.; Kander, R. G.; Velikov, V.; Chu, B.; Hsiao, B. S.; Marand, H., preprint.
(26) Lovinger, A. J.; Hudson, S. D.; Davis, D. D. *Macromolecules* **1992**, *25*, 1752.
(27) Marand, H.; Prasad, A. *Macromolecules* **1992**, *25*, 1731.
(28) Jonas, A.; Legras, R. *Polymer* **1991**, *32*, 2691.
(29) Jonas, A.; Legras, R. In *Advanced Thermoplastic Composites*; Kausch, H.-H., Ed.; Carl Hanser Verlag: Munich, 1993; p 57.
(30) Gehrke, R.; Riekel, C.; Zachmann, H. G. *Polymer* **1989**, *30*, 1582.
(31) Holdsworth, P. J.; Turner-Jones, A. *Polymer* **1971**, *12*, 195.
(32) Daoust, D.; Devaux, J.; Godard, P.; Jonas, A.; Legras, R. In *Advanced Thermoplastic Composites*; Kausch, H.-H., Ed.; Carl Hanser Verlag: Munich, 1993; p 3.
(33) Russell, T. P. In *Handbook on Synchrotron Radiation*; Brown, G., Moncton, D. E., Eds.; Elsevier Science Publishers, 1991; Vol. 3, p 379.
(34) Koberstein, J. T.; Morra, B.; Stein, R. S. *J. Appl. Crystallogr.* **1980**, *13*, 34.
(35) Strobl, G. R.; Schneider, M. *J. Polym. Sci., Polym. Phys. Ed.* **1980**, *18*, 1343.
(36) Zoller, P.; Kehl, T.; Starkweather, H. W.; Jones, G. A. *J. Polym. Sci., Part B: Polym. Phys.* **1989**, *27*, 993.
(37) Brandrup, J.; Immergut, E. H. *Polymer Handbook*, 3rd ed.; Wiley: New York, 1989.
(38) Jonas, A.; Legras, R.; Scherrenberg, R.; Reynaers, H. *Macromolecules* **1993**, *26*, 526.
(39) Blundell, D. J.; D'Mello, J. *Polymer* **1991**, *32*, 304.
(40) Hoffman, J. D.; Davies, G. T.; Lauritzen, J. I. In *Treatise on Solid-State Chemistry*; Hannay, N. B., Ed.; Plenum: New York, 1976; Vol. 3, p 497.
(41) Armitstead, K.; Goldbeck-Wood, G. *Adv. Polym. Sci.* **1992**, *100*, 219.
(42) Huo, P.; Cebe, P. *Macromolecules* **1992**, *25*, 902.
(43) Jonas, A.; Legras, R. *Macromolecules* **1993**, *26*, 813.
(44) Jonas, A., unpublished results.
(45) Cakmak, M.; Teitge, A.; Zachmann, H. G.; Whilte, J. L. *J. Polym. Sci., Part B: Polym. Phys.* **1993**, *31*, 371.
(46) Velikov, V.; Vivirito, J.; Marand, H. *Bull. Am. Chem. Soc.* **1994**, *39*, 168.
(47) Jonas, A.; Legras, R. *Macromolecules* **1993**, *26*, 2674.
(48) Cowley, J. M. *Diffraction Physics*, 2nd ed.; North Holland: Amsterdam, 1981.
(49) Jonas, A.; Legras, R. In *Advanced Thermoplastic Composites*; Kausch, H.-H., Ed.; Carl Hanser Verlag: Munich, 1993; p 83.
(50) Lovinger, A. J.; Davis, D. D. *J. Appl. Phys.* **1985**, *58*, 2843. Lovinger, A. J.; Davis, D. D. *Macromolecules* **1986**, *19*, 1861.
(51) Yoda, O. *Polym. Commun.* **1985**, *26*, 16.

MA950600W